($P = 0.0081$). The FS was also significantly lower in the conventional EPI treatment group (Fig. 5).

Discussion

NC-6300 was constructed to enhance antitumor activity and to reduce the adverse effects of EPI.[21] Previous data clearly showed that NC-6300 possessed superior antitumor activity to conventional EPI in mice bearing MDA-MB-231 human breast s.c. tumor.[21] In the present study, NC-6300 (10 or 15 mg/kg) also exerted significantly superior antitumor activity to EPI (10 mg/kg) both in s.c. HCC Hep3B xenografts and in the orthotopic liver tumor model. From the present pharmacokinetic analysis, we hypothesize that NC-6300 selectively accumulates in tumor tissue owing to the enhanced permeability and retention effect and directly reaches the cancer cells in order to attack them. Alternatively, the formulation spontaneously disintegrates while it is retained within the tumor tissue. Disintegrated EPI-bound unimers immediately reach and enter cancer cells. Then, under the acidic conditions in lysosomes, EPI is released to kill the cancer cells.

In terms of available preclinical data, the most prominent show that NC-6300 was found to cause marked reduction in the cardiotoxicity of conventional EPI. This was evaluated by precise echocardiography during and after a total of nine treatments with NC-6300 or EPI. The present pharmacokinetic study showed that the AUC value of released EPI in the heart was 36.2 μg h/g when NC-6300 (10 mg/kg) was given. The AUC value of EPI in the heart was 66.9 μg h/g in the case of conventional EPI treatment. The ratio of the AUC of EPI released from NC-6300 to that of native EPI was 0.54. In addition, the heart C_{max} of EPI was remarkably higher in the case of conventional EPI compared with NC-6300 treatment. In the echocardiographic examination, mice treated with conventional EPI showed significantly deteriorated EF and FS. In contrast, no mice treated with NC-6300 experienced cardiotoxicity in terms of EF and FS. Combining the results of the pharmacokinetic study and echocardiography, NC-6300 was found to markedly reduce cardiotoxicity. Among the various kinds of anticancer agents used in a clinical context, anthracyclines are one of the most important and commonly used drug groups in oncology.[9–13] Like other anticancer agents, drugs categorized into the anthracyclines have several adverse effects, including bone marrow toxicity, gastrointestinal toxicity, general fatigue, and hair loss. The most problematic adverse effect of the anthracyclines is undoubtedly cardiotoxicity[14–17] because, different from other adverse effects, it cannot be predicted when this cardiotoxicity will occur and how serious it will be. Furthermore, cardiotoxicity is occasionally unmanageable by any medical treatment. Although EPI has been developed in order to reduce the cardiotoxicity of DXR, EPI is still associated with serious cardiotoxicity.[18] However, the present data on NC-6300 suggest its potential to resolve this difficult clinical problem.

In the present preclinical study, NC-6300 appeared to show a strong antitumor effect in HCC xenografts compared with EPI. Furthermore, NC-6300 was found to reduce the cardiotoxicity of EPI markedly. Data from the present study warrant a clinical evaluation of NC-6300.

Acknowledgments

This work was supported by the Funding Program for World-Leading Innovative R&D on Science and Technology (FIRST Program) (Y.M.), the National Cancer Center Research and Development Fund (Y.M.), and the Ministry of Health, Labor and Welfare, Health and Labour Science Research Grants, Third Term Comprehensive Control Research for Cancer (Y.M.). We thank Mrs K. Shiina for her secretarial assistance.

Disclosure Statement

NanoCarrier Co. Ltd holds the patent for NC-6300 (Japanese patent number 4781435). M. Harada and H. Saito are the inventors of the product. NanoCarrier Co. Ltd received licensing fees from Kowa Co. Ltd (Nagoya, Japan) according to the license agreement.

References

1 El-Serag HB, Rudolph KL. Hepatocellular carcinoma: epidemiology and molecular carcinogenesis. *Gastroenterology* 2007; **132**: 2557–76.
2 Ferlay J, Shin HR, Bray F *et al.* Estimates of worldwide burden of cancer in 2008: GLOBOCAN 2008. *Int J Cancer* 2010; **127**: 2893–917.
3 Hung H. Treatment modalities for hepatocellular carcinoma. *Curr Cancer Drug Targets* 2005; **5**: 131–8.
4 Johnson PJ. Hepatocellular carcinoma: is current therapy really altering outcome? *Gut* 2002; **51**: 459–62.
5 Takayama T, Makuuchi M, Hirohashi S *et al.* Early hepatocellular carcinoma as an entity with a high rate of surgical cure. *Hepatology* 1998; **28**: 1241–6.
6 Llovet JM, Ricci S, Mazzaferro V *et al.* Sorafenib in advanced hepatocellular carcinoma. *N Engl J Med* 2008; **359**: 378–90.
7 Nowak AK, Chow PK, Findlay M. Systemic therapy for advanced hepatocellular carcinoma: a review. *Eur J Cancer* 2004; **40**: 1474–84.
8 Cheng AL, Kang YK, Chen Z *et al.* Efficacy and safety of sorafenib in patients in the Asia-Pacific region with advanced hepatocellular carcinoma: a phase III randomised, double-blind, placebo-controlled trial. *Lancet Oncol.* 2009; **10**: 25–34.
9 Llovet JM, Bruix J. Systematic review of randomized trials for unresectable hepatocellular carcinoma: chemoembolization improves survival. *Hepatology* 2003; **37**: 429–42.
10 Biganzoli L. Doxorubicin and paclitaxel versus doxorubicin and cyclophosphamide as first-line chemotherapy in metastatic breast cancer: The European Organization for Research and Treatment of Cancer 10961 Multicenter Phase III Trial. *J Clin Oncol* 2002; **20**: 3114–21.
11 Martin M, Rodriguez-Lescure A, Ruiz A *et al.* Randomized phase 3 trial of fluorouracil, epirubicin, and cyclophosphamide alone or followed by Paclitaxel for early breast cancer. *J Natl Cancer Inst* 2008; **100**: 805–14.
12 Roche H, Fumoleau P, Spielmann M *et al.* Sequential adjuvant epirubicin-based and docetaxel chemotherapy for node-positive breast cancer patients: the FNCLCC PACS 01 Trial. *J Clin Oncol* 2006; **24**: 5664–71.
13 Cunningham D, Starling N, Rao S *et al.* Capecitabine and oxaliplatin for advanced esophagogastric cancer. *N Engl J Med* 2008; **358**: 36–46.
14 Bristow MR, Billingham ME, Mason JW *et al.* Clinical spectrum of anthracycline antibiotic cardiotoxicity. *Cancer Treat Rep* 1978; **62**: 873–9.
15 Lefrak EA, Pitha J, Rosenheim S *et al.* A clinicopathologic analysis of adriamycin cardiotoxicity. *Cancer* 1973; **32**: 302–14.
16 Lipshultz SE, Alvarez JA, Scully RE. Anthracycline associated cardiotoxicity in survivors of childhood cancer. *Heart* 2008; **94**: 525–33.
17 Singal PK, Iliskovic N. Doxorubicin-induced cardiomyopathy. *N Engl J Med* 1998; **339**: 900–5.
18 de Azambuja E, Paesmans M, Beauduin M *et al.* Long-term benefit of high-dose epirubicin in adjuvant chemotherapy for node-positive breast cancer: 15-year efficacy results of the Belgian multicentre study. *J Clin Oncol* 2009; **27**: 720–5.
19 Salvatorelli E, Menna P, Lusini M *et al.* Doxorubicinolone formation and efflux: a salvage pathway against epirubicin accumulation in human heart. *J Pharmacol Exp Ther* 2009; **329**: 175–84.
20 Innocenti F, Iyer L, Ramirez J *et al.* Epirubicin glucuronidation is catalyzed by human UDP-glucuronosyltransferase 2B7. *Drug Metab Dispos* 2001; **29**: 686–92.
21 Harada M, Bobe I, Saito H *et al.* Improved anti-tumor activity of stabilized anthracycline polymeric micelle formulation, NC-6300. *Cancer Sci* 2011; **102**: 192–9.
22 Matsumura Y, Maeda H. A new concept for macromolecular therapeutics in cancer chemotherapy: mechanism of tumoritropic accumulation of proteins and the antitumor agent smancs. *Cancer Res* 1986; **46**: 6387–92.

SCIENTIFIC REPORTS

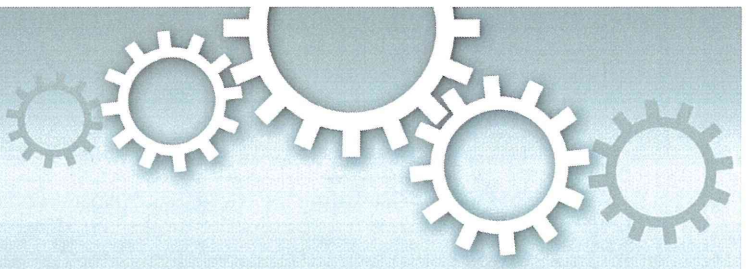

OPEN

SUBJECT AREAS:
CNS CANCER
RADIONUCLIDE IMAGING
THROMBOSIS
COAGULATION SYSTEM

Received
1 July 2013

Accepted
22 August 2013

Published
6 September 2013

Correspondence and requests for materials should be addressed to Y.M. (yhmatsum@east.ncc.go.jp)

* These authors contributed equally to this work.

Discovery of an uncovered region in fibrin clots and its clinical significance

Yohei Hisada[1,2]*, Masahiro Yasunaga[1]*, Shingo Hanaoka[3], Shinji Saijou[3], Takashi Sugino[4], Atsushi Tsuji[5], Tsuneo Saga[5], Kouhei Tsumoto[6], Shino Manabe[7], Jun-ichiro Kuroda[8], Jun-ichi Kuratsu[8] & Yasuhiro Matsumura[1,2]

[1]Division of Developmental Therapeutics, Research Centre for Innovative Oncology, National Cancer Centre Hospital East, 6-5-1 Kashiwanoha, Kashiwa, Chiba 277–8577, Japan, [2]Department of Integrated Biosciences, Graduate School of Frontier Sciences, The University of Tokyo, 5-1-5 Kashiwanoha, Kashiwa, Chiba 277–8561, Japan, [3]Project group, Biomatrix Research, Inc., 105 Higashifukai, Nagareyama, Chiba 270–0101, Japan, [4]Division of Pathology, Shizuoka Cancer Centre, 1007 Shimonagakubo, Nagaizumi, Sunto-gun, Shizuoka 411–8777, Japan, [5]Diagnostic Imaging Program, Molecular Imaging Centre, National Institute of Radiological Sciences, 4-9-1 Anagawa, Inage-ku, Chiba 263–8555, Japan, [6]Medical Proteomics Laboratory, Institute of Medical Science, The University of Tokyo, 4-6-1 Shirokanedai, Minato-ku, Tokyo 108–8639, Japan, [7]Synthetic Cellular Chemistry Laboratory, RIKEN Advanced Science Institute, 2-1 Hirosawa, Wako, Saitama 351–0198, Japan, [8]Department of Neurosurgery, Faculty of Medical and Pharmaceutical Sciences, Kumamoto University, 1-1-1 Honjo, Kumamoto, Kumamoto 860–0811, Japan.

Despite the pathological importance of fibrin clot formation, little is known about the structure of these clots because X-ray and nuclear magnetic resonance (NMR) analyses are not applicable to insoluble proteins. In contrast to previously reported anti-fibrin monoclonal antibodies (mAbs), our anti-fibrin clot mAb (clone 102–10) recognises an uncovered region that is exposed only when a fibrin clot forms. The epitope of the 102–10 mAb was mapped to a hydrophobic region on the Bβ chain that interacted closely with a counterpart region on the γ chain in a soluble state. New anti-Bβ and anti-γ mAbs specific to peptides lining the discovered region appeared to bind exclusively to fibrin clots. Furthermore, the radiolabelled 102–10 mAb selectively accumulated in mouse spontaneous tumours, and immunohistochemistry using this mAb revealed greater fibrin deposition in World Health Organization (WHO) grade 4 glioma than in lower-grade gliomas. Because erosive tumours are apt to cause micro-haemorrhages, even early asymptomatic tumours detected with a radiolabelled 102-10 mAb may be aggressively malignant.

Fibrinogen is composed of two pairs of polypeptide chains, including the Aα, Bβ, and γ chains, linked by disulfide bonds. Fibrinogen is involved in fibrin clot formation, which is the end result of blood coagulation[1–4]. Fibrin clot formation is the most dynamic and important event in haemostasis and thrombosis, which accompany injury[5], heart[6] or brain[7] infarction, severe inflammation[8], and cancer invasion[9] or metastasis[10].

Tumours that are erosive are also more destructive and thus result in fibrin clot formation. When cancer clusters erode adjacent normal or tumour vessels, micro-haemorrhage may occur, and fibrin clots are immediately formed in situ to stop the bleeding. These fibrin clots are subsequently replaced by collagenous stroma, similar to the process of normal wound healing[11]. Therefore, the "malignant cycle of blood coagulation" has been postulated to generate versatile cancer stroma, leading to cancer invasion into vessels, haemorrhage, fibrin clot formation, and replacement with collagenous tissue. Additionally, most human tumours possess abundant stroma[12,13], in contrast to human haematologic malignancies and tumour xenografts in mice, which have less interstitial tissue. Generally, more invasive cancers possess more abundant cancer stroma, most likely due to frequent haemorrhages at many places within or adjacent to the tumour tissue. In an invasive cancer, fibrin clot formation persists asymptomatically as long as cancer cells survive and expand from a tiny tumour to the advanced stage[12,13].

Results

To develop our anti-human fibrin mAb, we crushed a human fibrin clot and injected the suspension in saline into mice[13]. Consequently, we obtained a monoclonal antibody (mAb) (clone 102–10) that could distinguish fibrin clots from fibrinogen, soluble fibrin (precursor of fibrin clot[14]), and D-dimer (degradation product of fibrin clot[15]), which are all soluble proteins (Fig. 1a and Supplementary Fig. 1a). Although some anti-fibrin mAbs have been developed, none react exclusively with fibrin clots; rather, they also react with fibrinogen, soluble fibrin, or

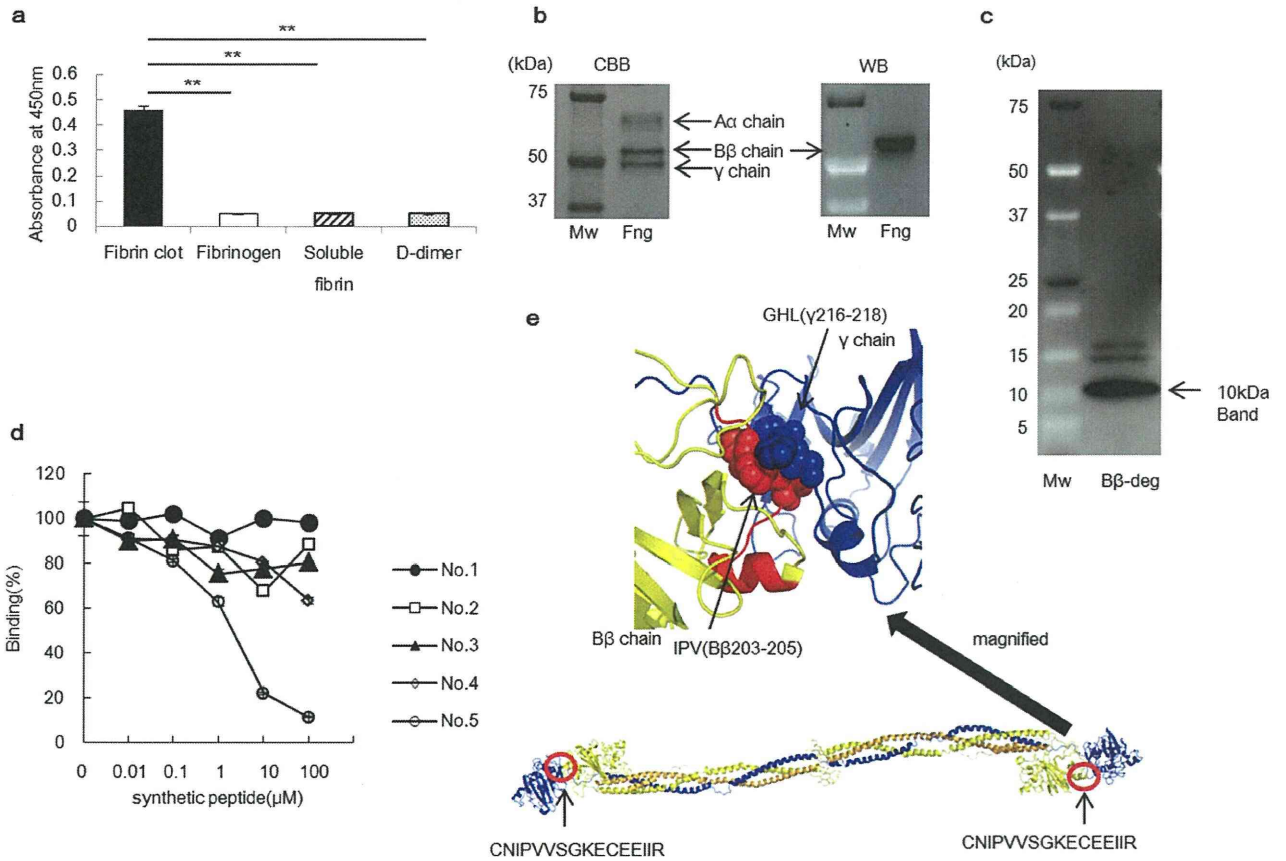

Figure 1 | Characterisation of the 102–10 mAb. (a) The 102–10 mAb was reactive to fibrin clots only ($n = 6$). The results are presented as the means ± s.d., ** $P < 0.01$. (b) Comparing CBB staining with western blot, the 102–10 mAb reacted exclusively with the Bβ chain of denatured whole fibrinogen (Fng). (c) Western blot was conducted for a sample of the digested Bβ chain, and all positive bands detected with the 102–10 mAb are shown. The amino acid sequence of the 10-kDa peptide detected by the 102–10 mAb was analysed in the next step. (d) Only the No. 5 peptide inhibited the binding of 102–10 mAb to fibrin clots ($n = 3$; $P < 0.01$, No. 4 vs. No. 5). (e) The epitope of 102–10 (Bβ201–216; red) interacted with the γ chain (blue), and Bβ203–205 (red ball) interacted with the region around γ216–218 (blue ball) in a hydrophobic manner. The whole structure of fibrinogen is shown (lower panel).

D-dimer[2,16–21]. Thus, the generation of a mAb that can distinguish fibrin clots from fibrinogen, soluble fibrin, and D-dimer represents a major breakthrough because these proteins share common amino acid sequences. The specificity of the 102–10 mAb differed from existing anti-fibrin mAbs (NYB-T2G1[22,23] and MH-1[20]), as the 102–10 mAb reacted only with fibrin clots (Supplementary Fig. 1b). Enzyme-linked immunosorbent assay (ELISA) also demonstrated that the 102–10 mAb specifically reacted with the fibrin clot in a dose-dependent manner, whereas it did not react with fibrinogen or D-dimer (Supplementary Fig. 1c).

Epitope mapping for the 102–10 mAb revealed that it reacted with fibrinogen under reducing and heat-denatured conditions in ELISA and western blot assays (Supplementary Fig. 1d–e). This result indicated that the epitope was exposed under reducing conditions. Comparing Coomassie brilliant blue (CBB) staining with the western blot results revealed that only the Bβ chain of fibrinogen reacted with the 102–10 mAb (Fig. 1b). To confirm the location of the epitope of the 102–10 mAb, the fibrinogen Bβ chain was digested with lysyl endopeptidase, and a Bβ chain derived peptide of approximately 10 kDa was obtained, which was recognised by the 102–10 mAb (Fig. 1c). According to the protein sequence result, this obtained peptide consisted of residues 149–234 of the Bβ chain. To confirm the epitope's sequence, five synthetic peptides were prepared with the following regions corresponding to synthetic peptides: No. 1 (Bβ149–178), No. 2 (Bβ179–208), No. 3 (Bβ209–234), No. 4 (Bβ171–186), and No. 5 (Bβ201–216). Competitive inhibition tests revealed that only one of these peptides (No. 5) inhibited the binding of the 102–10 mAb to fibrin clots, as measured by ELISA (Fig. 1d). The sequence of the No. 5 synthetic peptide was CNIPVVSGKECEEIIR, which constitutes a hydrophobic region of residues 201–216 of the Bβ chain. In view of the structure of fibrinogen, we could deduce that the epitope of the 102–10 mAb interacted with residues 206–220 of the γ chain of fibrinogen (Fig. 1e: Protein Data Bank (PDB) code 3GHG[24]). Interestingly, these 2 amino acid sequences are completely conserved in mammals, birds, amphibians, and fish (Basic Local Alignment Search Tool (BLAST)), which suggests that these sites have major importance for blood coagulation across species.

Identifying the epitope on a fibrin clot is generally difficult because X-ray analysis and NMR are not applicable to insoluble proteins. However, we identified the precise peptide sequence of the epitope using the 102–10 mAb against the fibrin clot and discovered a unique region in which certain sequences on the Bβ chain (containing the epitope of the 102–10 mAb) and γ chains of fibrinogen were hidden. To confirm this finding, we prepared a peptide antigen corresponding to the epitope region of the 102–10 mAb and a peptide antigen corresponding to the counterpart region on the γ chain. We immunised mice with these 2 synthetic peptides and succeeded in establishing mAbs against these regions on the Bβ chain (anti-Bβ mAb) and the γ chain (anti-γ mAb). Both the anti-Bβ mAb and the

anti-γ mAb specifically recognised fibrin clots (Fig. 2a–b). These findings imply that a conformational change occurs in the region that acts as an epitope for each mAb when fibrinogen develops into a fibrin clot, which produces the unique region (Fig. 2c). To characterise this unique region, a competition ELISA was conducted using the peroxidase-conjugated anti-Bβ mAb, peroxidase-conjugated anti-γ mAb, and each corresponding cold mAb. The binding of peroxidase-conjugated anti-Bβ mAb to the fibrin clot was blocked by the cold anti-Bβ mAb but not by the cold anti-γ mAb. Moreover, the binding of peroxidase-conjugated anti-γ mAb to the fibrin clot was blocked by the cold anti-γ mAb but not by the cold anti-Bβ mAb (Supplementary Fig. 2). These findings indicate that the newly identified unique region within fibrin clots was large enough for both the anti-Bβ and anti-γ mAbs to bind simultaneously (Fig. 2d). Further structural analysis of this unique region revealed that hydrophobic interactions and ionic and hydrogen bonds are involved in the interaction between the Bβ chain and γ chain of this particular region (Fig. 2e–g). The dynamic force exerted upon the formation of a fibrin clot is expected to break these bonds, resulting in the appearance of the unique region within the clots.

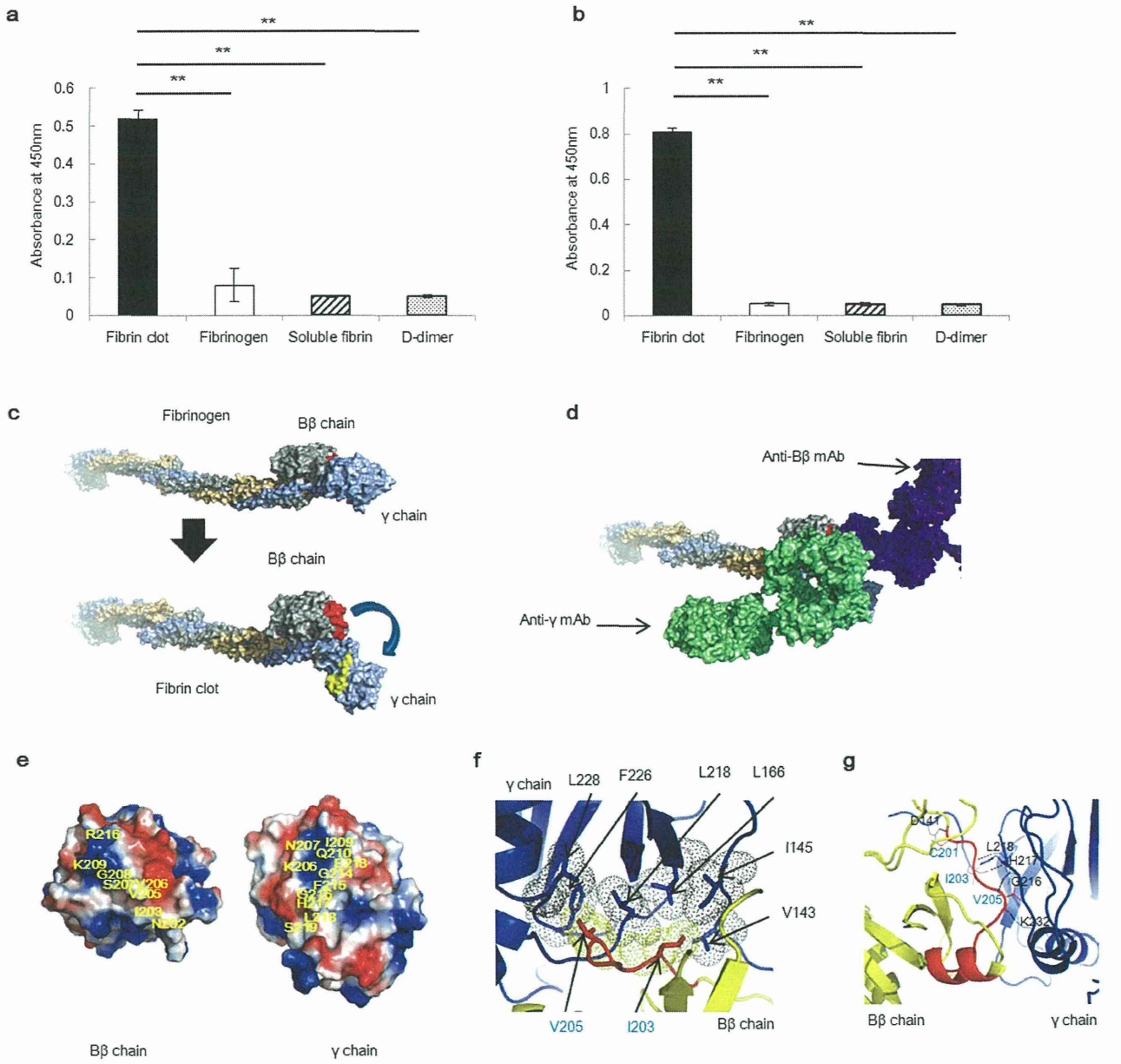

Figure 2 | Discovery of a unique region in fibrin clots. Hydrophobic, ionic, and hydrogen bonds were detected between the Bβ chain and γ chain in the unique region. (a) The anti-Bβ mAb and (b) anti-γ mAb were reactive only to fibrin clots ($n = 8$). The results are presented as the means ± s.d., ** $P < 0.01$. (c) Image of the structural change that occurred as fibrinogen transformed into a fibrin clot; the unique region was formed only when fibrinogen transformed into a fibrin clot (blue arrow). The epitope of the 102–10 mAb (red) on the Bβ chain (silver) and residues 206–220 (yellow) of the γ chain (light blue) were the components of the unique region. (d) The unique region within the fibrin clot was proposed to be large enough for both mAbs to bind to the region simultaneously. (e) Electrostatic surface representations (−5 kT/e, red, to +5 kT/e, blue) of the Bβ chain and γ chain in the unique region. Yellow characters indicate the epitope of the 102–10 mAb and the counterpart on the γ chain. (f) Hydrophobic interaction between the Bβ chain (yellow dots) and γ chain (black dots) of the unique region. (g) Amino acids (blue characters) on the Bβ chain (yellow) and amino acids (black characters) on the γ chain (blue) form hydrogen bonds in the epitope region. (f, g) Red indicates the epitope of 102–10.

Because this uncovered region is uncovered only when a fibrin clot forms and the amino acid sequence of the epitope of the 102–10 mAb is completely conserved in mammals, the 102–10 mAb and other mAbs developed against human fibrin clots cross-reacted with mouse or rat fibrin clots. Therefore, we investigated the fate of fibrin clots in mice or rats using disease models, such as models of cerebral infarction, incisional wounds, and arthritis (Fig. 3a). These results indicated that fibrin clot formation occurred only in the acute phase of non-malignant diseases, including thrombosis, inflammation, and trauma, and these clots virtually disappeared within 2 to 3 weeks and were substituted by collagen in the late phase. We next synthesised a positron emission tomography (PET) probe of ^{89}Zr-labelled 102–10 (Fig. 3b), which was injected into mice bearing chemically induced spontaneous cutaneous tumours generated using 7,12-dimethylbenz[a]anthracene (DMBA) as an initiator and phorbol 12-myristate 13-acetate (PMA) as a promoter[25]. This spontaneous tumour was selected as an appropriate experimental model to evaluate our immuno-probe because it exhibits remarkable fibrin deposition and abundant interstitial tissue, similar to clinical human cancers and unlike human tumour xenografts in mice[26]. The 102–10 mAb probe showed clear and more specific accumulation in tumours compared to cetuximab (control), as assessed by computerized tomography (CT) scan (Fig. 3c, Supplementary Fig. 3). Next, we histologically evaluated the specificity of the 102–10 mAb probe within the tumour tissue. Haematoxylin and eosin (HE) staining showed that the tumour consisted of areas with basophilic tumour cells and eosinophilic tumour stroma, and the accumulation of the 102–10 mAb probe was more pronounced in fibrin clot-positive

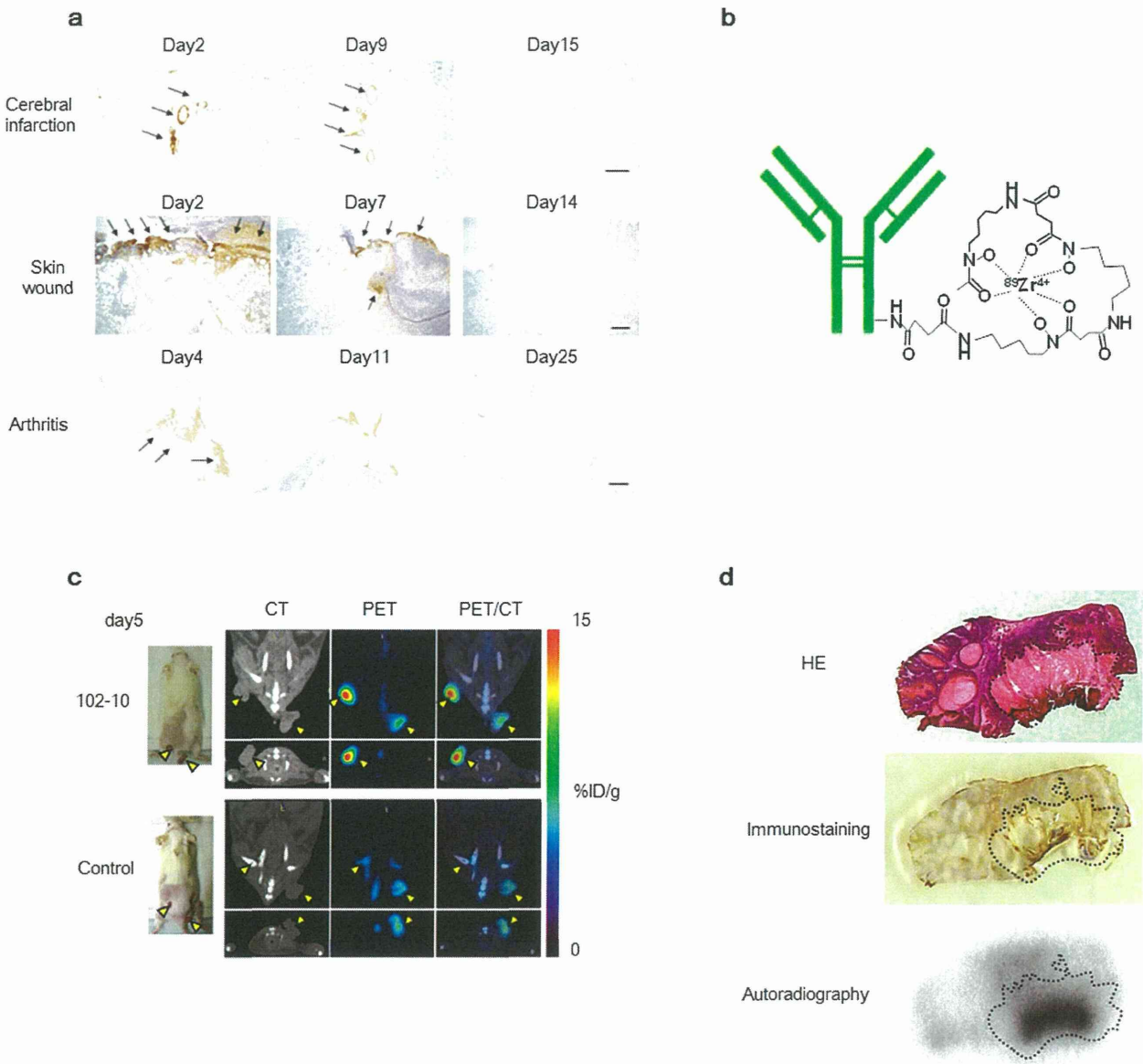

Figure 3 | The kinetics of fibrin clot deposition in several non-malignant disease models and PET/CT with ^{89}Zr-labelled 102–10 in spontaneous tumour models. (a) The kinetics of fibrin clot deposition in rat cerebral infarction (upper), mouse incisional wound (middle), and mouse arthritis (lower) were evaluated immunohistochemically. Fibrin clot deposition was observed at the acute phase (left and middle) but not at the late phase (right). Scale bar, 100 μm. (b) The PET probe was composed of the 102–10 mAb, a linker, and ^{89}Zr. (c) The ^{89}Zr-labelled 102–10 mAb probe showed clearer and more specific accumulation in tumours as compared to the control (cetuximab). The yellow arrows indicated tumours. (d) The 102–10 mAb probe accumulated within fibrin-positive tumour stroma, as represented by the dashed line.

tumour stroma (Fig. 3d). These PET/CT data from mouse experiments can be reasonably extrapolated to humans because the 102–10 mAb can recognise both human and mouse fibrin clots, and humans and mice show common features of fibrin deposition.

To evaluate the reactivity of the 102–10 mAb to intravital fibrin clots under various conditions in humans, normal tissue and tissues from non-malignant and malignant diseases were stained with the 102–10 mAb. Strong fibrin deposition was observed in almost all cancer tissues, including brain, lung, pancreatic, and colorectal cancers, but not in normal tissues (Fig. 4a and Supplementary Table 1). In cases of non-malignant disease, fibrin clots were detected at the onset of cerebral infarction and cardiac infarction or in cases of serious inflammation, such as acute pancreatitis (Supplementary Table 1). However, no clear fibrin clots were detected in the late or chronic phases of non-malignant conditions following the digestion of fibrin clots by plasmin and replacement by collagenous tissue (Fig. 4b).

Erosive types of cancer are known to be more destructive, resulting in higher fibrin clot deposition. In this context, we closely investigated fibrin deposition in surgically resected samples of glioma, one of the most erosive tumour types. Immunohistochemistry was conducted for WHO-classified glioma tissue samples, and the level of fibrin deposition was graded into three subgroups: (−) fibrin clot not detectable, (+) faint but clear deposition, or (++) strong heterogeneous or diffuse deposition (Fig. 4c). Fibrin deposition was observed in 100% (20/20) of grade 4 gliomas (glioblastoma multiforme (GBM)), with strong fibrin deposition observed in 65% of cases (13/20). In grade 3 gliomas, fibrin deposition was observed in 40% of cases (8/20), with strong fibrin deposition observed in 10% of cases (2/20). In grade 1/2 gliomas, fibrin deposition was observed in 60% of cases (12/20), and strong fibrin deposition was observed in 10% of cases (2/20) (Fig. 4d).

Discussion

Combining previous lines of clinicopathological evidence with our present data, even tiny and asymptomatic tumours will likely become aggressively malignant if they are detected by PET/CT using the radiolabelled 102–10 mAb. The deposition of fibrin in non-malignant disease is inevitably accompanied by various symptoms related to the particular pathology, such as infarction or inflammation. Conversely, tumour-related fibrin deposition is not associated with any symptoms, even in patients with stage 4 disease. When a cancer diagnosis is accompanied by symptoms, such as pain or macroscopic bleeding, the cancer likely involves sensory nerves and the destruction of bone and large blood vessels, which is generally observed in patients with end-stage cancer. Therefore, earlier detection of cancers at the asymptomatic stage using mAbs is important to achieve a favourable clinical outcome[27].

The biological significance of tumour fibrin clots has been gradually elucidated, as several growth factors that preserve the fibrin matrix have been shown to promote tumour cell growth, angiogenesis[28], and metastasis[27,29]. Conversely, the role of fibrin clots in the tumour stroma has yet to be definitively characterised. Here, we discovered an uncovered region that develops in the fibrin clot during its formation, and we generated mAbs that bound exclusively to fibrin clots. The specificity of the 102–10 mAb to fibrin clots was verified by the present ELISA and western blot (Figure 1a,

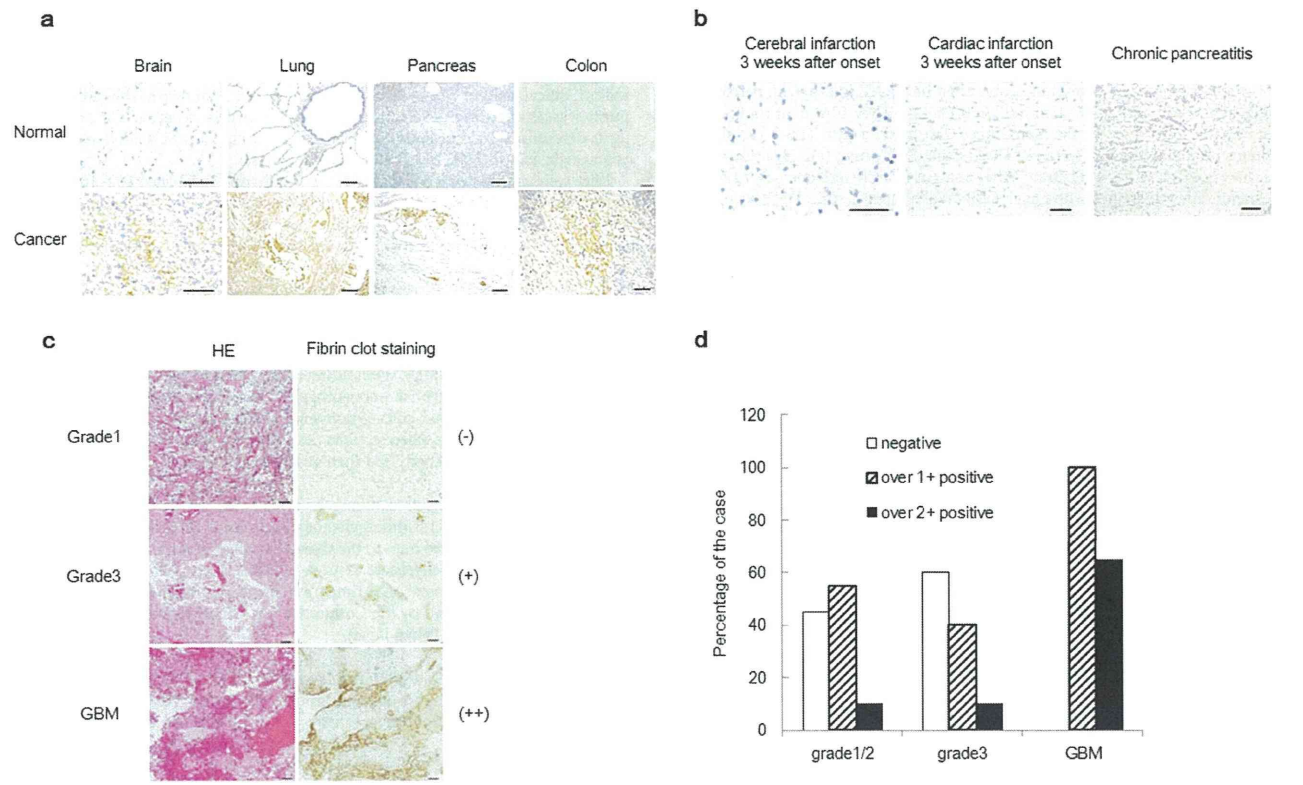

Figure 4 | Immunostaining of fibrin clots in various human tissues and the fibrin clot status according to WHO-classified glioma grade. (a, b) Fibrin deposition was strongly detected in human cancer tissues but not in normal human tissues or during the late or chronic phases of non-malignant diseases. Scale bar, 100 μm. (c) Immunohistochemical analysis of glioma. The left panels show HE staining, and the right panels show fibrin clot staining. The level of fibrin deposition was graded into 3 subgroups: (−) undetectable fibrin clot (upper panel, grade1); (+) faint but clear deposition (middle panel, grade3); or (++) strong heterogeneous or diffuse deposition (lower panel, GBM). (d) The percentage of fibrin deposition is shown. The clinical stages of the patients were classified as grade 1/2, grade 3, or grade 4 (GBM) according to the WHO grade classification. Each group consisted of 20 cases.

supplementary Fig. 1c, and 4). Therefore, the 102–10 mAb may not be neutralised by fibrinogen, soluble fibrin, or D-dimer in the bloodstream due to its unique properties.

Our immunohistochemical and PET/CT findings using these newly developed anti-insoluble-fibrin mAbs, including 102–10, further demonstrated that these mAbs could be used to detect high-grade, aggressive, malignant tumours. Further development of such a method to detect fibrin clots is therefore desirable from an oncological perspective.

Methods

Production of the 102–10 mAb. We developed our anti-human fibrin mAb by converting fibrinogen (Sigma, St Louis, MO) into a fibrin clot via thrombin (Sigma) cleavage. The fibrin was frozen in liquid nitrogen and crushed, and the crushed fibrin was then suspended in saline and used to immunise mice. Lymph node cells from an immunised mouse were fused with myeloma cells (P3U1), and specific antibody-producing hybridoma clones were selected by ELISA as described previously[13].

Enzyme-linked immunosorbent assay (ELISA). The reference standards for soluble fibrin and D-dimer were obtained from Sekisui Medical (Tokyo, Japan). One microgram of antigen was immobilised onto a 96-well plate for 12 hours. The fibrinogen-immobilised plates were then treated with a thrombin solution at 37°C for 1 hour to prepare the fibrin clot plates, as described previously[20]. The wells were then blocked using N102 (Nichiyu, Tokyo, Japan) for 3 hours. Subsequently, the plates were incubated in 1 μg/mL peroxidase-conjugated mAb 1 hour, and the wells were washed with Tris-buffered saline (TBS) containing 0.05% Tween 20 (TBS-T). Finally, the mAbs bound to the wells were visualised using a 1-Step Slow TMB-ELISA (Thermo, Waltham, MA, USA) as a substrate for 30 minutes.

Western blot. The mAbs were first conjugated to peroxidase (Dojindo, Kumamoto, Japan). One microgram of fibrinogen or its proteolytic product sample was obtained by Sodium dodecyl sulphate polyaclylamide gel electrophoresis (SDS-PAGE) under reducing, heat-shocked, or untreated conditions. The proteins were then electrophoretically transferred to polyvinylidenedifluoride (PVDF) membranes (Bio-Rad, Hercules, CA, USA) using the Trans-Blot Turbo transfer machine (Bio-Rad). The membranes were then placed in a protein detection system (SNAP i.d.; Millipore, Billerica, MA, USA) and blocked with phosphate-buffered saline (PBS) containing 0.3% Difco skim milk (Becton Dickinson, Franklin Lakes, NJ, USA) and 0.1% Tween 20 (PBS-T, Sigma). The membranes were then incubated in 2 μg/mL peroxidase-conjugated mAbs with 0.3% skim milk in 0.1% PBS-T for 10 min at room temperature. Subsequently, the membranes were washed with TBS-T. Finally, the proteins on the membrane were visualised using ECL prime (GE Healthcare, Piscataway, NJ, USA) as a substrate. After analysis in a ChemiDoc imager (Bio-Rad), the membrane was stained with Quick CBB (Wako Pure Chemical Industries, Osaka, Japan).

Isolation of fibrinogen Bβ chain. Five micrograms of fibrinogen were separated by SDS-PAGE under reducing conditions. The polyacrylamide gel was then stained with EZ Stain reverse (ATTO, Tokyo, Japan). The fibrinogen Bβ chain fraction was cut out from the polyacrylamide gel, followed by extraction of the protein using an Atto prep MF column (ATTO).

Limited digestion with lysyl endopeptidase and protein sequencing. Lysyl endopeptidase (Wako Pure Chemical Industries) digestion of the fibrinogen Bβ chain protein was carried out in PBS (pH 7.4) with a protein:enzyme ratio (w/w) of 45 : 1 at 37°C for 6 hours, and the digested peptide was separated by SDS-PAGE electrophoresis under reducing conditions. The fragments were detected by western blot, and the minimum positive band (approximately 10 kDa) was obtained using the method described above. The amino acid sequence of the 10-kDa peptide was determined using a PPSQ-33A protein sequencer (Shimadzu, Kyoto, Japan).

Inhibition of 102–10 binding to fibrin clots using a series of synthetic peptides. Five synthetic peptides [No. 1 (Bβ149–178), No. 2 (Bβ179–208), No. 3 (Bβ209–234), No. 4 (Bβ170–186), and No. 5 (Bβ201–216)] were prepared using the amino acid sequence of the 10-kDa peptide (Sigma). A PBS solution containing 1 μg/mL peroxidase-conjugated 102–10 was then mixed with diluted synthetic peptides (0.01–100 μM), and the mixture was incubated for 1 hour at 37°C. After discarding the blocking reagent, 100 μL of the mixture was applied to a fibrin-coated 96-well plate[17]. Subsequently, the wells were washed with TBS-T, and the antibodies in the wells were visualised using the 1-Step Slow TMB ELISA as a substrate for 5 minutes.

Producing the anti-Bβ chain and anti-γ chain mAbs. The crystal structure of fibrinogen (3GHG) was obtained from the RCSB Protein Data Bank (http://www.rcsb.org/pdb/home/home.do) and visualised using PyMOL ver1.3r1 edu (http://www.pymol.org/pymol). To produce new antibodies that recognise epitope regions of the fibrin clot Bβ chain (CNIPVVSGKECEEIIR) or γ chain (KNWIQYKEGFGHLSP), recombinant epitope protein was produced from pET21b (Novagen, Darmstadt, Germany) and fibrinogen Bβ chain DNA or fibrinogen γ chain DNA (Origene Technology, Rockville, MD). Six-week-old BALB/cAnNCrlCrlj mice (Charles River Japan, Yokohama, Japan) were immunised intraperitoneally (i.p.) with an emulsion of Freund's complete adjuvant (DIFCO, Franklin Lakes, NJ, USA) and a saline solution containing 50 μg of the Bβ chain of the epitope peptide with a 4M-tag (Bio Matrix Research, Inc., Chiba, Japan). Three to five successive booster injections were administered i.p. at 2-week intervals using the same amount of antigen in an adjuvant system (Sigma). A final boost was provided by administering the same amount of antigen intravenously. An antibody recognising the γ chain of the fibrin clot was produced by ITM Co. Ltd (Matsumoto, Japan). The specificity of the obtained mAbs against the epitope regions of the Bβ and γ chains was evaluated by ELISA.

Hydrophobic, ionic, and hydrogen bonds between the Bβ chain and γ chain in the unique region of fibrin clots. Electrostatic surface representations (−5 kT/e, red, to +5 kT/e, blue) of the Bβ chain and γ chain were generated using the APBS software package (https://sites.google.com/a/poissonboltzmann.org/software/apbs), and the images of all molecular structures were displayed in PyMOL ver1.3r1 edu.

Immunohistochemistry. Non-malignant human tissues were obtained from Fukushima Medical University. Glioma samples were obtained from Kumamoto University. Immunohistochemical studies in human tissue samples were conducted on surgically resected tissue samples and tissue samples obtained from autopsy. All samples were collected according to an institutional review board-approved protocol. Tissue sections from paraffin-embedded tissue samples were prepared, and heat-induced antigen retrieval was performed at 120°C for 10 minutes in 10 mM citrate (pH 6). After blocking with 5% skim milk in PBS, the sections were incubated with the 102–10 mAb for 1 to 2 hours at room temperature or overnight at 4°C. After washing with PBS, the sections were then incubated with peroxidase-conjugated anti-human IgG secondary antibody (MBL Co., Ltd., Nagoya, Japan) for 60 minutes. The reaction was visualised using DAB (Dako, Glostrup, Denmark), and the slides were counterstained with haematoxylin.

PET/CT imaging and autoradiography using ^{89}Zr-labelled 102–10. The 102–10 mAb was conjugated to *p*-isothiocyanatobenzyl-desferrioxamine B (DF) as previously described[30]. The conjugation ratio of DF to IgG was estimated to be 1.0 to 1.3, as determined by size-exclusion chromatography using a PD10 column (GE Healthcare). The nonconjugated chelate was removed using a Sephadex G-50 spin column (GE Healthcare). ^{89}Zr-oxalate was produced using a cyclotron at the National Institute of Radiological Sciences (Chiba, Japan) as previously described[31]. The DF-conjugated 102–10 mAb (100 μg in 20 μL of PBS) was incubated with 5.0 to 5.6 MBq of ^{89}Zr-oxalate (3.7–5.6 GBq/mL, pH 7–9) for 1 hour at room temperature. The radiolabelled 102–10 mAb was purified using a Sephadex G-50 spin column. The radiochemical yield of ^{89}Zr-labelled IgG was between 73 and 96%, the radiochemical purity was between 96 and 98%, and the specific activity was between 37 and 44 kBq/μg as determined by thin-layer chromatography using 50 mM diethylene triamine pentaacetic acid (DTPA, pH 7) as the mobile phase.

Mice were injected with approximately 3.7 MBq of ^{89}Zr-labelled 102–10 mAb into the tail vein. The injected protein dose was adjusted to 100 μg per mouse by the addition of unlabelled antibody. The PET data were acquired for 10 to 20 minutes using a small-animal PET system (Inveon, Munich, Germany) under isoflurane anaesthesia. Body temperature was maintained at 37°C using a lamp and a heating pad during the scan. The images were reconstructed using 3D maximum a posteriori (18 iterations with 16 subsets, β = 0.2 resolution) without attenuation correction. The tracer uptake was expressed as the percentage of the injected dose per gram of tissue (% ID/g). After PET scanning, the CT images were acquired with an X-ray source set at 90 kVp and 200 μA using a small-animal CT system (R_mCT2, Rigaku, Tokyo, Japan). After imaging, the mice were euthanised, and the tumours were excised and quickly frozen in an optimal-cutting-temperature (OCT) compound (Sakura Finetek Japan, Tokyo, Japan). The dried sections (20 μm thick) were exposed to an imaging plate (Fuji Film, Tokyo, Japan) and then stained with HE.

Animal model. Chemical skin carcinogenesis was induced as previously described[26,32–34]. Briefly, 7,12-dimethylbenz[a]anthracene (DMBA; 250 μg/mL in acetone; Sigma) was applied once to the shaved dorsal skin of the mice as an initiator. After 1 week, phorbol 12-myristate 13-acetate (PMA; 25 μg/mL in acetone; Sigma) was applied weekly (for a total of 32 times) as a promoter. All animal procedures and experiments were approved by the Committee for Animal Experimentation of the National Cancer Centre, Tokyo Japan.

Statistical analysis. A two-sided Student's *t*-test was used to compare the two groups. Steel's test was used to compare multiple groups with Statcel3 (OMS, Saitama, Japan). A two-factor factorial analysis of variance was used to evaluate the inhibition effect.

1. Mosesson, M. W. Fibrinogen and fibrin structure and functions. *J Thromb Haemost* **3**, 1894–1904 (2005).
2. Pacella, B. L., Jr., Hui, K. Y., Haber, E. & Matsueda, G. R. Induction of fibrin-specific antibodies by immunization with synthetic peptides that correspond to amino termini of thrombin cleavage sites. *Mol Immunol* **20**, 521–527 (1983).
3. Brass, E. P., Forman, W. B., Edwards, R. V. & Lindan, O. Fibrin formation: the role of the fibrinogen-fibrin monomer complex. *Thromb Haemost* **36**, 37–48 (1976).
4. Graeff, H., Hafter, R. & von Hugo, R. On soluble fibrinogen-fibrin complexes. *Thromb Res* **16**, 575–576 (1979).

5. Drew, A. F., Liu, H., Davidson, J. M., Daugherty, C. C. & Degen, J. L. Wound-healing defects in mice lacking fibrinogen. *Blood* **97**, 3691–3698 (2001).
6. Silvain, J. *et al.* Composition of coronary thrombus in acute myocardial infarction. *Journal of the American College of Cardiology* **57**, 1359–1367 (2011).
7. Skaf, E. *et al.* Venous thromboembolism in patients with ischemic and hemorrhagic stroke. *Am J Cardiol* **96**, 1731–1733 (2005).
8. Levi, M., van der Poll, T. & Buller, H. R. Bidirectional relation between inflammation and coagulation. *Circulation* **109**, 2698–2704 (2004).
9. Idell, S. *et al.* Regulation of fibrin deposition by malignant mesothelioma. *Am J Pathol* **147**, 1318–1329 (1995).
10. Im, J. H. *et al.* Coagulation facilitates tumour cell spreading in the pulmonary vasculature during early metastatic colony formation. *Cancer Res* **64**, 8613–8619 (2004).
11. Dvorak, H. F. Tumors: wounds that do not heal. Similarities between tumour stroma generation and wound healing. *N Engl J Med* **315**, 1650–1659 (1986).
12. Matsumura, Y. Cancer stromal targeting (CAST) therapy. *Adv Drug Deliv Rev* **64**, 710–719 (2012).
13. Yasunaga, M., Manabe, S. & Matsumura, Y. New concept of cytotoxic immunoconjugate therapy targeting cancer-induced fibrin clots. *Cancer Sci* **102**, 1396–1402 (2011).
14. Soe, G., Kohno, I., Inuzuka, K., Itoh, Y. & Matsuda, M. A monoclonal antibody that recognizes a neo-antigen exposed in the E domain of fibrin monomer complexed with fibrinogen or its derivatives: its application to the measurement of soluble fibrin in plasma. *Blood* **88**, 2109–2117 (1996).
15. Wada, H. *et al.* Elevated levels of soluble fibrin or D-dimer indicate high risk of thrombosis. *J Thromb Haemost* **4**, 1253–1258 (2006).
16. Laudano, A. P. & Doolittle, R. F. Synthetic peptide derivatives that bind to fibrinogen and prevent the polymerization of fibrin monomers. *Proc Natl Acad Sci U S A* **75**, 3085–3089 (1978).
17. Kudryk, B., Rohoza, A., Ahadi, M., Chin, J. & Wiebe, M. E. A monoclonal antibody with ability to distinguish between NH2-terminal fragments derived from fibrinogen and fibrin. *Mol Immunol* **20**, 1191–1200 (1983).
18. Scheefers-Borchel, U., Muller-Berghaus, G., Fuhge, P., Eberle, R. & Heimburger, N. Discrimination between fibrin and fibrinogen by a monoclonal antibody against a synthetic peptide. *Proc Natl Acad Sci U S A* **82**, 7091–7095 (1985).
19. Schielen, W. J., Voskuilen, M., Tesser, G. I. & Nieuwenhuizen, W. The sequence A alpha-(148-160) in fibrin, but not in fibrinogen, is accessible to monoclonal antibodies. *Proc Natl Acad Sci U S A* **86**, 8951–8954 (1989).
20. Gargan, P. E., Graffney, P. J., Pleasants, J. R. & Ploplis, V. A. A Monoclonal Antibody which Recognises an Epitopic Region Unique to the Intact Fibrin Polymeric Structure. *Fibrinolysis* **7**, 275–283 (1993).
21. Hui, K. Y., Haber, E. & Matsueda, G. R. Monoclonal antibodies to a synthetic fibrin-like peptide bind to human fibrin but not fibrinogen. *Science* **222**, 1129–1132 (1983).
22. Kudryk, B., Rohoza, A., Ahadi, M., Chin, J. & Wiebe, M. E. Specificity of a monoclonal antibody for the NH2-terminal region of fibrin. *Mol Immunol* **21**, 89–94 (1984).
23. Rosebrough, S. F. *et al.* Aged venous thrombi: radioimmunoimaging with fibrin-specific monoclonal antibody. *Radiology* **162**, 575–577 (1987).
24. Kollman, J. M., Pandi, L., Sawaya, M. R., Riley, M. & Doolittle, R. F. Crystal structure of human fibrinogen. *Biochemistry* **48**, 3877–3886 (2009).
25. Filler, R. B., Roberts, S. J. & Girardi, M. Cutaneous two-stage chemical carcinogenesis. *CSH Protoc* **2007**, pdb prot4837 (2007).
26. Hirakawa, S. *et al.* VEGF-A induces tumour and sentinel lymph node lymphangiogenesis and promotes lymphatic metastasis. *The Journal of experimental medicine* **201**, 1089–1099 (2005).
27. Prandoni, P., Falanga, A. & Piccioli, A. Cancer and venous thromboembolism. *Lancet Oncol* **6**, 401–410 (2005).
28. Fernandez, P. M., Patierno, S. R. & Rickles, F. R. Tissue factor and fibrin in tumour angiogenesis. *Semin Thromb Hemost* **30**, 31–44 (2004).
29. Palumbo, J. S. *et al.* Fibrinogen is an important determinant of the metastatic potential of circulating tumour cells. *Blood* **96**, 3302–3309 (2000).
30. Perk, L. R. *et al.* p-Isothiocyanatobenzyl-desferrioxamine: a new bifunctional chelate for facile radiolabeling of monoclonal antibodies with zirconium-89 for immuno-PET imaging. *Eur J Nucl Med Mol Imaging* **37**, 250–259 (2010).
31. Nagatsu, K. *et al.* An alumina ceramic target vessel for the remote production of metallic radionuclides by in situ target dissolution. *Nuclear medicine and biology* **39**, 1281–1285 (2012).
32. Takano, K., Tatlisumak, T., Bergmann, A. G., Gibson, D. G., 3rd. & Fisher, M. Reproducibility and reliability of middle cerebral artery occlusion using a silicone-coated suture (Koizumi) in rats. *J Neurol Sci* **153**, 8–11 (1997).
33. Hutamekalin, P. *et al.* Collagen antibody-induced arthritis in mice: development of a new arthritogenic 5-clone cocktail of monoclonal anti-type II collagen antibodies. *J Immunol Methods* **343**, 49–55 (2009).
34. Basu, A., Kligman, L. H., Samulewicz, S. J. & Howe, C. C. Impaired wound healing in mice deficient in a matricellular protein SPARC (osteonectin, BM-40). *BMC Cell Biol* **2**, 15 (2001).

Acknowledgments

This work was supported by the National Cancer Centre Research and Development Fund (Y.M.); the Funding Program for World-Leading Innovative R&D in Science and Technology (FIRST Program) (Y.M.); the Third Term Comprehensive Control Research for Cancer from the Ministry of Health, Labour, and Welfare of Japan (Y.M.); a Grant-in-Aid for Scientific Research or Priority Areas from the Ministry of Education, Culture, Sports, Science, and Technology; the Princess Takamatsu Cancer Research Fund (Y.M.); and the Japanese Foundation for Multidisciplinary Treatment of Cancer (Y.M.). We thank Dr. S. Iwanaga for his expertise. We also thank Ms. M. Takigahira for her assistance with the animal experiments, Mrs. H. Koike and Mrs. M. Araake-Mizoguchi for their assistance with producing the 102–10 mAb, and Mrs. K. Shiina for secretarial support.

Author contributions

Y.M. provided the original concept for the research and the anti-fibrin clot monoclonal antibody (102–10). Y.H., M.Y. and Y.M. designed the study. Y.H., M.Y., S.H., S.S., T.S., T.S. and A.T. performed the experiments. Y.H., M.Y., S.H., S.S., T.S., A.T., T.S., K.T., S.M., J.K., J.K. and Y.M. discussed the results and wrote the paper.

Additional information

Supplementary information accompanies this paper at http://www.nature.com/scientificreports

Competing financial interests: The authors declare no competing financial interests.

How to cite this article: Hisada, Y. *et al.* Discovery of an uncovered region in fibrin clots and its clinical significance. *Sci. Rep.* **3**, 2604; DOI:10.1038/srep02604 (2013).

Chapter 6
Cancer Stromal Targeting (CAST) Therapy and Tailored Antibody Drug Conjugate Therapy Depending on the Nature of Tumor Stroma

Yasuhiro Matsumura, Masahiro Yasunaga, and Shino Manabe

Abstract In spite of recent success of monoclonal antibody (mAb) drug conjugate (ADC) therapy in patients with hypervascular and special tumors recognized by a particular mAb, there are several issues to be solved for ADC counted as universal therapy for any types of cancer. Especially most human solid tumors possess abundant stroma that hinders the distribution of ADC. To overcome these drawbacks, we developed a unique strategy that the cancer stromal targeting (CAST) therapy by cytotoxic immunoconjugate bound to the collagen IV or fibrin network in the tumor stroma from which the payload is released gradually and distributed throughout the tumor, resulting in the arrest of tumor growth due to induced damage to tumor cells and tumor vessels.

In addition to the CAST therapy, we clarified the appropriate combination of targeting antibody and conjugate design of antitumor immunoconjugate depending on a quantity of tumor stroma. Hence, we selected two types of conjugate linker, ester bond and carbamate bond. It was found that combination of stromal targeting mAb and a linker composed of ester bond to release drug outside the cells was effective against the stroma-rich cancer. Conversely, cancer cell targeting via carbamate bond to release drug inside the cells was effective against stroma-poor cancer. It seemed that outcome of ADC therapy against each individual tumor having distinct stromal structure was dependent on the selection of conjugation design, as well as targeting mAb.

Y. Matsumura, M.D., Ph.D. (✉) • M. Yasunaga
Division of Developmental Therapeutics, National Cancer Center Hospital East, Kashiwa, Chiba, Japan
e-mail: yhmatsum@east.ncc.go.jp

S. Manabe
Synthetic Cellular Chemistry Laboratory, RIKEN, Wako, Saitama, Japan

Y.H. Bae et al. (eds.), *Cancer Targeted Drug Delivery: An Elusive Dream*,
DOI 10.1007/978-1-4614-7876-8_6,

Introduction

There are two main concepts in DDS, active targeting and passive targeting. Active targeting involves monoclonal antibodies (mAb) or ligands to tumor-related receptors which can target the tumor by utilizing the specific binding ability between the antibody and antigen or between the ligand and its receptor. The passive targeting system can be achieved by the EPR effect, that is, the enhanced permeability and retention effect [1–3]. Small molecules easily leak from normal vessels in the body, which gives small molecules a short plasma half-life. On the other hand, macromolecules have a long plasma half-life because they are too large to pass through the normal vessel walls, unless they are trapped by the reticuloendothelial system (RES) in various organs. Solid tumors generally possess several pathophysiological characteristics: hypervasculature, secretion of vascular permeability factors stimulating extravasation of macromolecules within a tumor, and absence of effective lymphatic drainage from tumors that impedes the efficient clearance of macromolecules accumulated in solid tumor tissues.

Macromolecules and lipids in the interstitial tissue are known to be recovered via the lymphatics in normal tissues [4]. The limited recovery from the lymphatic system in tumor tissues may be attributed to poor development of the lymphatics in tumor tissues, which has been demonstrated by using lipid lymphographic agents [5].

Although there is no clear anatomical proof that tumor lymphogenesis is implicated in the drainage of extravasated macromolecules in human, some studies have indicated that the growth of lymphatic vessels is actively involved in tumor dissemination [6].

This inconsistency regarding tumor lymphogenesis may be due to differences between mice and humans, or differences among tumor types. These characteristics of solid tumors are the EPR effect. Based on the EPR effect, several formulations categorized in passive targeting have been developed and some of them such as Doxil [7] and Abraxane [8] have been approved in clinical use, and anticancer agents (ACAs) incorporating micelles and polymer-conjugated ACAs are now under preclinical and clinical evaluation [9–11].

Monoclonal antibody, which can target the tumor cell actively by the specific binding ability against corresponding antigen, easily extravasates from leaky tumor vessels but not from normal vessels, is long retained in the tumor by utilizing active targeting and passive targeting based on the EPR effect. Therefore, numerous mAbs have been developed and conjugated with ACAs or toxins to create "ADC, immunoconjugate strategy" [12–15]. Recent examples of the conjugates include anti-CD33-calicheamicin and anti-CD20-radiolabeled immunoconjugate and were effective to hematological malignancy such as malignant lymphoma and leukemia [12]. Very recently, the phase 3 trial showed that T-DM1 appeared to have a significant survival benefit in HER2-positive breast cancer that is a representative of hypervascular cancers [16]. Heterogeneity of the cancer cells, however, prevents development of the ADC based on cell-specific antigen [17–20]. Moreover, conventional ADCs depend on cleavage of conjugation site with intracellular biochemical (enzymatic) process after the cell uptake of the conjugate [21–24]. In addition to

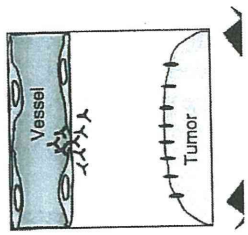

Fig. 6.1 The schema of ar
barrier like malignant lym
internalized after antigen-b
cer (PC) possess stromal b
cells such that antigen-bind

such annoying characte
such as pancreatic can
the distribution of mA
developed a unique str
cytotoxic immunoconju
stroma from which the
tumor, resulting in the
and tumor vessels [29,
immunoconjugate ther
tumor stroma were not

In this context, it is
antibody and conjugate
tity of tumor stroma. I
and carbamate bond. \
mAb and a linker comp
effective against the st
carbamate bond to rele
poor cancer. It seemed
vidual tumor having d
conjugation design, as